Nano Energy 57 (2019) 405–413

Contents lists available at ScienceDirect

Nano Energy

journal homepage: www.elsevier.com/locate/nanoen

Full paper

An $In_{0.42}Ga_{0.58}N$ tunnel junction nanowire photocathode monolithically integrated on a nonplanar Si wafer

Yongjie Wang[a], Srinivas Vanka[a,c], Jiseok Gim[b], Yuanpeng Wu[a], Ronglei Fan[a,d], Yazhou Zhang[a,e], Jinwen Shi[e], Mingrong Shen[d], Robert Hovden[b], Zetian Mi[a,*]

[a] Department of Electrical Engineering and Computer Science, University of Michigan, 1301 Beal Avenue, Ann Arbor, MI 48109, USA
[b] Department of Materials Science and Engineering, University of Michigan, 2300 Hayward Street, Ann Arbor, MI 48109, USA
[c] Department of Electrical and Computer Engineering, McGill University, 3480 University Street, Montreal, Quebec, Canada H3A 0E9
[d] College of Physics, Optoelectronics and Energy, Soochow University, 1 Shizi Street, Suzhou 215006, China
[e] International Research Center for Renewable Energy, State Key Laboratory of Multiphase Flow in Power Engineering, Xi'an Jiaotong University, 28 West Xianning Road, Xi'an 710049, China

ARTICLE INFO

Keywords:
Photocathode
Solar water splitting
InGaN
Nanowire
Tunnel junction

ABSTRACT

Group III-nitride semiconductors exhibit many ideal characteristics for solar water splitting, including a tunable energy bandgap across nearly the entire solar spectrum and suitable band edge positions for water oxidation and proton reduction under visible and near-infrared light irradiation. To date, however, the best reported energy conversion efficiency for III-nitride semiconductor photocathodes is still below 1%. Here we report on the demonstration of a relatively efficient *p*-type $In_{0.42}Ga_{0.58}N$ photocathode, which is monolithically integrated on an *n*-type nonplanar Si wafer through a GaN nanowire tunnel junction. The open pillar design, together with the nonplanar Si wafer can significantly maximize light trapping, whereas the tunnel junction reduces the interfacial resistance and enhances the extraction of photo-generated electrons. In addition, photodeposited Pt nanoparticles on InGaN nanowire surfaces significantly improve the cathodic performance. The nanowire photocathode exhibits a photocurrent density of 12.3 mA cm^{-2} at 0 V vs. RHE and an onset potential of 0.79 V vs. RHE under AM 1.5 G one-sun illumination. The maximum applied bias photon-to-current efficiency reaches 4% at ~0.52 V vs. RHE, which is one order of magnitude higher than the previously reported values for III-nitride photocathodes. Significantly, no performance degradation was measured for over 30 h solar water splitting with a steady photocurrent density ~12 mA cm^{-2} without using any extra surface protection, which is attributed to the spontaneous formation of N-terminated surfaces of InGaN nanowires to protect against photocorrosion.

1. Introduction

Solar water splitting and hydrogen generation is one important step of artificial photosynthesis to meet the increasing demand of clean, renewable energy [1]. An essential component of a solar water splitting device is a photocathode, often consisting of a *p*-type semiconductor, that can drive proton reduction efficiently and stably in acidic solution under sunlight illumination [2–4]. In the past decades, extensive efforts have been devoted to exploring various photocathode materials and structures. Illustrated in Fig. 1 are the energy band diagrams of some commonly studied photocathode semiconductors [5–10]. Metal oxide semiconductors typically have large energy bandgap values and, as a consequence, can only absorb a small portion of the solar spectrum [11]. To utilize the majority energy of sunlight, Group III-V and IV semiconductors, including GaP, $GaInP_2$, GaAs, InP, and Si photocathode materials have been intensively studied. Although relatively high photocurrent densities have been reported, e.g. ~22 mA cm^{-2} for GaAs (E_g ~1.4 eV) [12], ~25 mA cm^{-2} for InP (E_g ~1.3 eV) [13], and ~35 mA cm^{-2} for n^+/p-Si (E_g ~1.1 eV) [14], these materials are not stable in acidic electrolytes, which is kinetically preferred for proton reduction. An extra protection layer, e.g. TiO_2, is therefore required to protect against detrimental photocorrosion [15,16]. In addition, there is an urgent need to develop a semiconductor photocathode with an energy bandgap ~1.7–2.0 eV, which, when integrated with a narrow bandgap ~1.1 eV bottom light absorber, e.g. Si, promises solar water splitting cells with a solar-to-hydrogen (STH) efficiency up to 30% [1,17–19].

In the quest for a 1.7–2.0 eV semiconductor material that can

* Corresponding author.
E-mail address: ztmi@umich.edu (Z. Mi).

https://doi.org/10.1016/j.nanoen.2018.12.067
Received 17 June 2018; Received in revised form 11 December 2018; Accepted 20 December 2018
Available online 21 December 2018
2211-2855/ © 2018 Published by Elsevier Ltd.

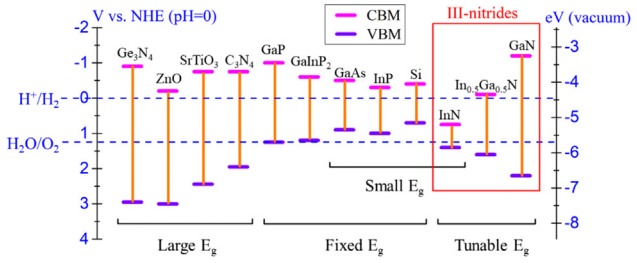

Fig. 1. Schematic energy band diagram of some commonly studied single-junction photocathode materials, including metal oxides, III-V, Si, and III-nitride semiconductors, assuming in acidic solution (pH = 0). CBM and VBM represent the conduction band minimum and valence band maximum, respectively.

function efficiently and stably as a photocathode in acidic electrolyte, group III-nitrides, e.g. GaN and its alloys, have drawn considerable attention [5,6,17]. GaN based semiconductors have been widely used in electronics and photonics industries, and they are the second most produced semiconductor material only next to Si. Significantly, InGaN with indium composition in the range of 40–50% exhibits a direct energy bandgap of 1.65–1.9 eV, whose band edges can straddle proton reduction and water oxidation potentials [5]. III-nitride semiconductors also exhibit large carrier mobility and a high absorption coefficient ($\sim 10^5\ cm^{-1}$) [20–24], and have demonstrated the capability to support current densities of hundreds of kA/cm^2 in power transistors [25–27] (e.g. six to seven orders of magnitude larger than that relevant for solar water splitting). To date, however, the best reported energy conversion efficiency for an InGaN photocathode in acidic electrolyte is still below 1% (see supplementary Table S1) [28–30]. Moreover, their long-term stability in an acidic electrolyte has remained largely unknown. The underlying challenges include the presence of large densities of defects and dislocations for conventional InGaN materials grown by metal-organic chemical vapor deposition (MOCVD) and the difficulty in achieving *p*-type doping of In-rich InGaN [31–34].

In this work, we have performed a detailed investigation of the synthesis and photoelectrochemical properties of crystalline In-rich *p*-type InGaN nanowire arrays on industry-grade non-planar Si wafers that are commonly used for fabricating commercial Si solar cell modules. The nanowires are synthesized using a plasma-assisted molecular beam epitaxy (MBE) method under N-rich conditions to promote the formation of N-terminated surfaces [35–38], which can protect against photocorrosion and oxidation. *p*-Type InGaN nanowires are connected with the underlying *n*-type Si wafer through a tunnel junction, which provides low-resistivity connection and further serve as an electron blocking layer to enhance electron extraction. For the InGaN photocathode with indium composition ~42% (E_g ~1.9 eV), a short-circuit photocurrent density of 12.3 mA cm^{-2} and a large onset potential of 0.79 V vs. RHE were measured. The maximum applied bias photon-to-current efficiency (ABPE) is 4% at ~0.52 V vs. RHE, which is more than one order of magnitude larger than that of previously reported InGaN photocathodes [28–30]. Significantly, the photocathode shows no degradation for over 30 h solar wafer splitting at a steady current density of 12 mA cm^{-2} without adding any extra surface protection layer. Detailed studies were also performed to correlate the photoelectrochemical performance with indium composition of the InGaN nanowires. Further improvement in the device performance, together with the integration with a buried Si junction, promises high-efficiency, stable unassisted solar water splitting systems [18].

2. Results and discussions

Schematically shown in Fig. 2a is the design of *p*-type InGaN nanowire photocathode formed on a non-planar Si wafer. Each nanowire consists of an *n*-type GaN segment (length ~160 nm), an n^{++}-GaN/InGaN/p^{++}-GaN tunnel junction, and a *p*-type InGaN segment (length ~800 nm). The top *p*-InGaN segment serves as the light absorber and photocatalytic reactor for proton reduction reaction. Pt nanoparticles are deposited on the nanowire surfaces using a photodeposition process (see Experimental section). The direct integration of *p*-type InGaN on Si wafer (whether *n*- or *p*-type) generally leads to high resistivity, due to the formation of extensive defects and impurity incorporation at the heterointerface. To alleviate this issue, an *n*-type GaN nanowire segment is first grown on *n*-type Si wafer, schematically shown in the inset of Fig. 2a, followed by the formation of an n^{++}/p^{++} GaN tunnel junction [39,40]. A thin layer of InGaN is also incorporated between n^{++} and p^{++}-GaN, illustrated in the inset of Fig. 2b. The piezoelectric field created by the InGaN segment can further reduce the depletion depth and resistivity of the tunnel junction, thereby enhancing the recombination of charge carriers (photo-generated holes from *p*-InGaN and electrons injected from *n*-Si) [41–43]. Such tunnel junction design has been previously exploited to realize efficient light emitting diodes (LEDs) and photoelectrodes in HBr splitting, but has not been used in solar water splitting [40,44,45]. It is important to note, however, that in the present study the InGaN segments are not uniformly incorporated in all nanowires due to the use of non-planar Si wafer.

Shown in Fig. 2b is the schematic energy band diagram along the growth direction of an ideal *p*-InGaN tunnel junction nanowire under illumination. The photocathode is connected to a platinum (Pt) counter electrode where water oxidation reaction takes place. Under light illumination, photo-excited holes are collected through tunnel junction, whereas photo-excited electrons migrate to the InGaN/liquid interface to drive proton reduction reaction due to the downward surface band bending, shown in Fig. 2b. The p^{++}-GaN also serves as an electron blocking layer to reflect photo-excited electrons, which can then readily migrate to InGaN nanowire surfaces, due to the downward surface band bending. Charge carrier extraction, which is often a bottleneck for conventional planar photoelectrodes, is no longer limited by carrier diffusion for the presented photocathode, due to the small size nanowires and large surface area [46].

InGaN tunnel junction nanowires are grown on non-planar Si wafers using a Veeco GenII MBE system equipped with a radio frequency plasma-assisted nitrogen source (see Experimental section). The non-planar Si wafer, shown in Fig. 2c, was created by using hot KOH solution (see Experimental section). The growth was conducted in N-rich conditions to promote the formation of nanowires with N-terminated surfaces. The use of non-planar Si wafer, together with the light trapping effect of nanowire arrays, can enhance light absorption [47–49]. The top-view scanning electron microscopy (SEM) image of InGaN nanowires grown on non-planar Si is shown in Fig. 2d. More detailed SEM images are shown in supplementary Fig. S1. Photoluminescence (PL) spectra measured at room temperature for InGaN nanowires are shown in Fig. 2e. By changing the growth conditions, the PL emission wavelengths can be varied from ~500 nm to ~750 nm, corresponding to an energy bandgap values of ~2.48 eV to ~1.65 eV, and indium compositions of ~24% to ~51%, respectively (see supplementary Fig. S2) [37,50,51]. Significantly, the band edges of such InGaN nanowires can straddle the water redox potentials, which is essentially required for unassisted solar water splitting [5]. It is also observed that, with increasing indium composition, the PL intensity becomes weaker and the linewidth becomes broader, indicating the reduced crystallinity and large compositional non-uniformity (see supplementary Fig. S3) [52]. A detailed correlation between the PEC performance and indium composition is discussed next.

Energy dispersive X-ray (EDX) mapping on the top plane of $In_{0.42}Ga_{0.58}N$ nanowires shows that the nanowires are composed of Ga, In, and N with the presence of Pt nanoparticles, as demonstrated in Fig. 3a and supplementary Fig. S4a. Displayed in Fig. 3b is the cross-sectional high angle annular dark-field scanning transmission electron microscopy (HAADF-STEM) image of $In_{0.42}Ga_{0.58}N$ nanowires, which reveals the crystalline InGaN nanowires (width ~200 ± 40 nm, height

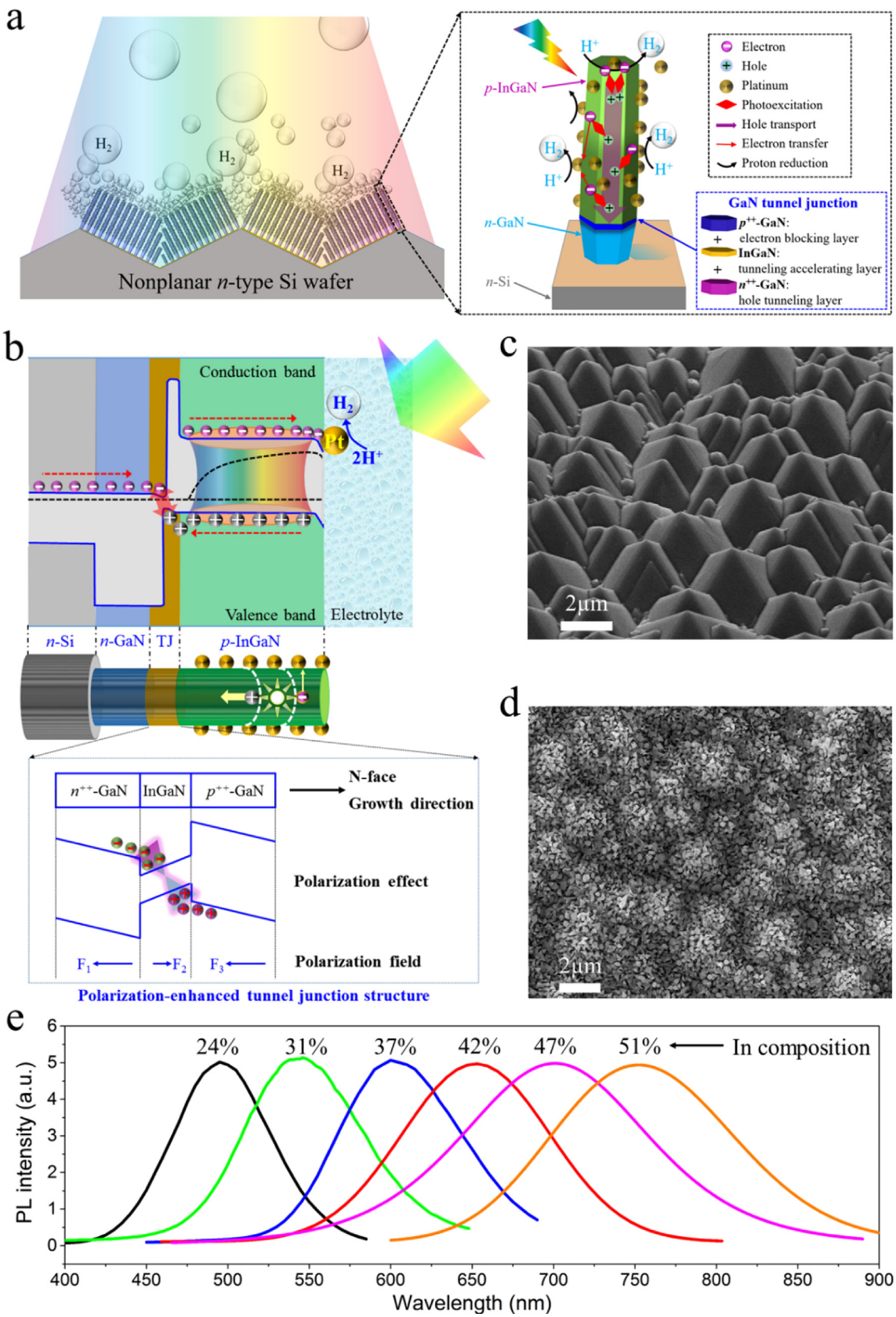

Fig. 2. Illustration and characterization of *p*-InGaN tunnel junction nanowire photocathode. (a) Schematic of proton reduction on *p*-InGaN nanowires on a nonplanar Si wafer. The detailed tunnel junction heterostructure and the processes of photo-excitation, hole collection through the tunnel junction, electron extraction, and proton reduction on Pt co-catalyst nanoparticles are shown in the inset. (b) Schematic energy band diagram of InGaN tunnel junction nanowires under illumination. The energy band diagram of a polarization-enhanced tunnel junction, n^{++}-GaN/InGaN/p^{++}-GaN, is shown in the inset. (c) SEM image of a non-planar silicon wafer surface. (d) Top-view SEM image of InGaN nanowires grown on non-planar Si wafer. (e) Room-temperature photoluminescence spectra of different InGaN nanowires, showing a large variation of the emission peaks from 500 to 750 nm.

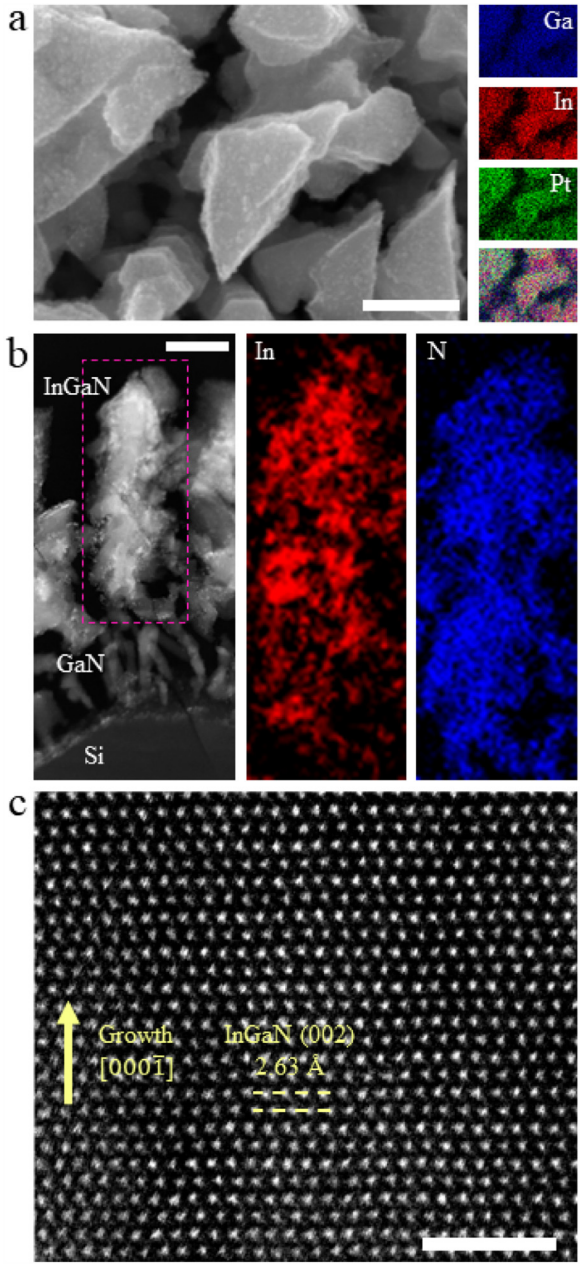

Fig. 3. Electron microscope characterization of Pt-decorated $In_{0.42}Ga_{0.58}N$ nanowires. (a) Top-view SEM image with EDX elemental mapping, where Ga-L, In-L, and Pt-M characteristic X-ray spectra were measured. Scale bar, 200 nm. (b) HAADF-STEM image of cross-sectional InGaN nanowires with simultaneous EELS mapping images of In and N atoms. Scale bar, 200 nm. (c) Atomic resolution HAADF-STEM image highlighting the crystalline lattice spacing consistent with InGaN crystal. Scale bar, 2 nm.

~800 nm, spacing ~800 ± 80 nm) extend atop an early growth of GaN nanowires. Using the characteristic X-rays obtained on pure GaN as a reference specimen, the elemental composition of InGaN was quantitatively estimated, showing that 62.7 ± 10.5% of Ga and 37.3 ± 10.5% of In are present in the InGaN nanowire. Fig. 3c shows the atomic structure within a InGaN nanowire and a lattice spacing of 2.63 Å corresponding to the InGaN (002) wurtzite lattice planes along the preferred < 0001 > growth direction (*c*-axis) [5]. Fast Fourier transform (FFT) patterns of the HAADF-STEM image exhibit InGaN (001) reflection peak which is a forbidden peak in electron diffraction pattern of wurtzite hexagonal symmetry (supplementary Fig. S5). The (001) reflection peak demonstrates the existence of periodic atomic ordering along the c-axis caused by a nonrandom atomic site occupancy of indium and gallium within the two unique cation sublattice positions ((0,0,0) and (1/3,2/3,1/2)) in a wurtzite unit cell [53]. This confirms the periodic ordering of In and Ga in the crystalline InGaN nanopillars.

In the low-dimensional geometry heteroepitaxy, increased In incorporation can occur due to the onset of strain relaxed growth [37]. The low substrate temperature (530–670 °C) and relatively high N_2 flow rate (1 sccm) used for InGaN growth combined with 1D nanowire geometry allow for effective strain relaxation and reduce phase separation. Furthermore, Pt co-catalysts with a size of 2–6 nm were uniformly loaded on InGaN nanowire surface to further enhance the performance, as demonstrated in Fig. 3 and supplementary Fig. S4. In some cross-sectional GaN tunnel junction nanowires, an InGaN segment (~ 5 nm) was confirmed on the top of the GaN nanowire by the occurrence of additional superlattice spots (001) and higher HAADF intensity associated with the heavier atomic weight of indium (supplementary Fig. S6). Our detailed studies further suggest that the thin InGaN segment is not uniformly incorporated in all GaN tunnel junction nanowires, which is likely due to the shadowing effects created by neighboring nanowires when grown on a non-planar Si wafer. This provides opportunities for further improving the device performance and yield. In addition, a thin SiN_x nanolayer is often formed at the Si and GaN interface, as previously reported by Eftychis et al. [54,55]. Further studies are needed to understand its effect on charge carrier transport during solar water splitting.

Photoelectrochemical measurements of *p*-InGaN tunnel junction nanowire photocathodes were performed in 0.5 M H_2SO_4 solution (pH ~0) under the illumination of 100 mW cm^{-2} simulated AM1.5 G solar spectrum (see Experimental section). The photocathodic behavior of *p*-InGaN/TJ/Si nanowires was first confirmed by performing Mott-Schottky measurement (see supplementary Fig. S7) [56–58]. Shown in Fig. 4a is the linear sweep voltammetry measurement of *p*-$In_{0.42}Ga_{0.58}N$ tunnel junction photocathode. The performance of *p*-InGaN/Si (without tunnel junction) measured under identical conditions is also shown for comparison. *p*-InGaN/Si (without tunnel junction) structures exhibit poor onset potential, ~0 V vs. RHE, and low current density, due to inefficient charge carrier separation and extraction. The performance of *p*-InGaN/Si (without tunnel junction) photocathode is also severely limted by the large interfacial resistance between *p*-InGaN and the underlying *n*-type Si substrate. The *p*-$In_{0.42}Ga_{0.58}N$ tunnel junction nanowire photocathode, on the other hand, exhibits dramatically improved PEC performance. The onset potential is 0.79 V vs. RHE, and a significantly enhanced photocurrent density of 12.3 mA cm^{-2} is measured at 0 V vs. RHE. The dark current density is negligible compared to the photocurrent, confirming the measured photocurrent comes from solar energy conversion. This is further confirmed under chopped light illumination (see supplementary Fig. S8). The substantially improved onset potential and photocurrent density of *p*-InGaN tunnel junction nanowire photocathode is directly related to the efficient charge separation, hole collection, and electron extraction enabled by the integration with GaN tunnel junction. In this study, we have only demonstrated InGaN tunnel junction nanowire integrated on a nonplanar Si wafer for efficient proton reduction reaction. However, planar Si wafer may also work to synthesize InGaN tunnel junction nanowire photocathode, by appropriate growth optimization.

We have further investigated the photoelectrochemical performance of *p*-InGaN tunnel junction nanowire photocathodes with indium compositions varying from ~24% to ~51%. The measured current densities at 0 V vs. RHE and onset potentials are plotted vs. the PL peak position of InGaN nanowires, shown in Fig. 4b. It is seen that the measured photocurrent (absolute value) first shows an increasing trend with indium incorporation from 24% to 42%, due to the reduced bandgap and more efficient light absorption. A significant reduction of photocurrent, however, was observed for indium concentration > 42%, which may be attributed to the increased defect formation and enhanced non-radiative recombination of In-rich InGaN. These

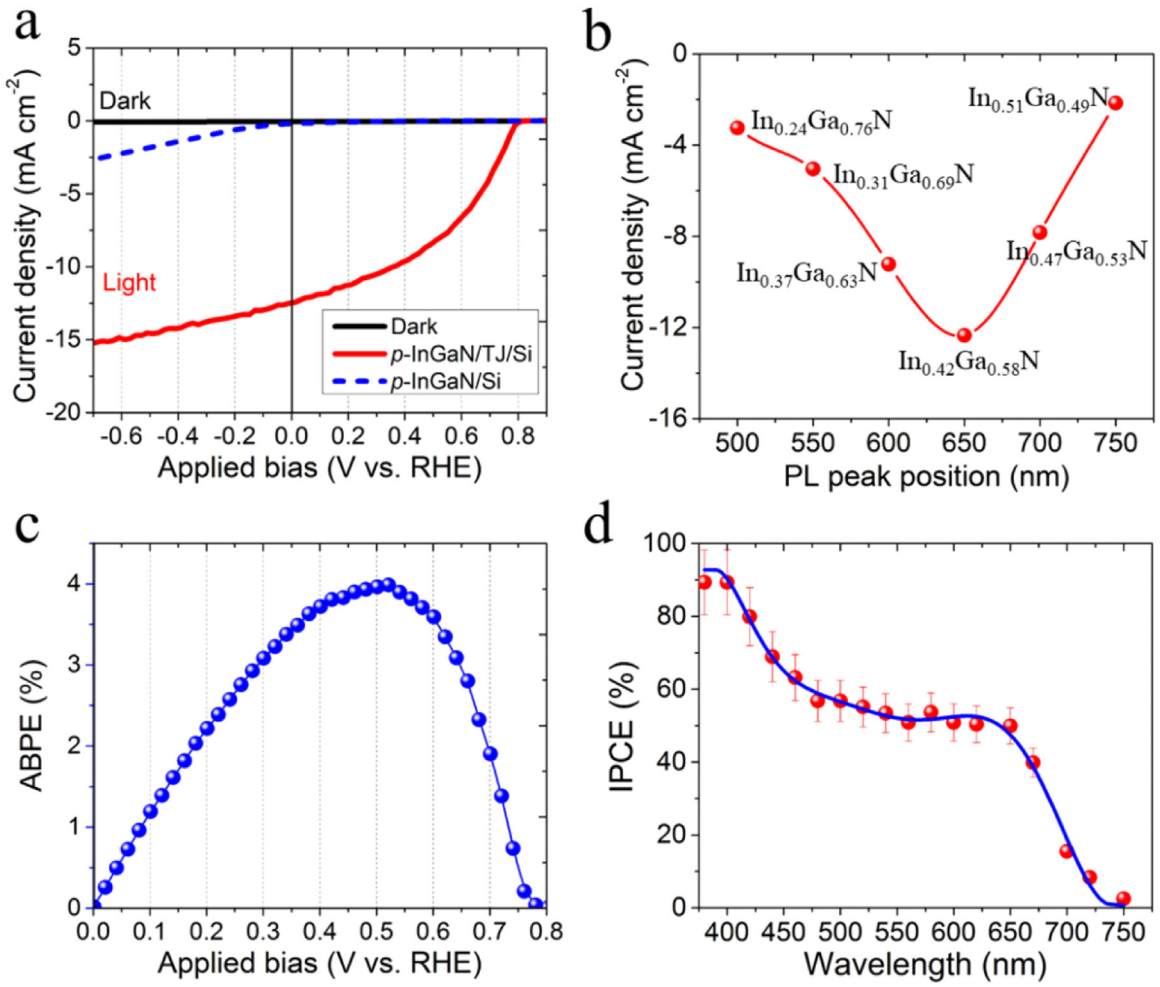

Fig. 4. Photoelectrochemical performance of *p*-InGaN tunnel junction nanowire photocathodes. (a) Linear sweep voltammetry measurements of *p*-$In_{0.42}Ga_{0.58}N$ tunnel junction nanowires (*p*-InGaN/TJ/Si) and *p*-$In_{0.42}Ga_{0.58}N$ without tunnel junction (*p*-InGaN/Si) in H_2SO_4 electrolyte (0.5 M, pH ~0) under stimulated AM 1.5 G solar illumination of 100 mW cm^{-2}. (b) Variations of the photocurrent density (measured at 0 V vs. RHE) vs. indium composition of *p*-InGaN tunnel junction nanowire photocathodes. (c) Variations of the applied-bias photon-to-current conversion efficiency (ABPE) for *p*-$In_{0.42}Ga_{0.58}N$ tunnel junction nanowire photocathode vs. the applied bias voltage (vs. RHE). (d) The incident photon-to-current conversion efficiency (IPCE) of *p*-$In_{0.42}Ga_{0.58}N$ tunnel junction nanowire photocathode measured at 0 V vs. RHE in 0.5 M H_2SO_4 solution. The solid blue curve is a polynomial fitting.

observations are consistent with the degradation of the optical properties for In-rich InGaN nanowires (see supplementary Fig. S3). Moreover, the significant reduction of measured photocurrent for In-rich InGaN nanowires may also be related to the poor nanowire morphology, shown in supplementary Fig. S12. The highest photocurrent density ~12.3 mA cm^{-2} was measured for *p*-InGaN nanowires with In composition ~42% (E_g ~1.9 eV). Its photoelectrochemical performance is shown in Fig. 4a.

The ABPE for the InGaN tunnel junction nanowire photocathode was derived using the following equation:

$$\mathrm{ABPE}(\%) = \frac{\textit{photocurrent}\ \text{density}(\mathrm{mA{\cdot}cm^{-2}}) \times \textit{applied}\ \text{bias}(\mathrm{V\ vs.\ RHE})}{100\ \mathrm{mW{\cdot}cm^{-2}}} \times 100\% \quad (1)$$

A maximum ABPE of 4% was measured at ~0.52 V vs. RHE, which is the highest value ever-reported for III-nitride semiconductor photocathodes (see supplementary Table S1). Fig. 4d shows the incident photon-to-current conversion efficiency (IPCE) of *p*-$In_{0.42}Ga_{0.58}N$ nanowire photocathode measured at 0 V vs. RHE in 0.5 M H_2SO_4 solution. IPCE reaches > 90% for light illumination < 400 nm, and then gradually decreases to 50–60% at 500–600 nm. Negligible IPCE is measured above 650 nm, which is consistent with the energy bandgap of $In_{0.42}Ga_{0.58}N$. The IPCE in the visible wavelength can be further improved by optimizing the epitaxy and properties of InGaN nanowires. By integrating the IPCE results with the standard AM 1.5 G spectrum, a maximum photocurrent density of 14.4 mA cm^{-2} is predicted (see supplementary Fig. S9), which agrees reasonably well with the measured saturation current density shown in Fig. 4a.

We have further performed continuous solar water splitting measurements on *p*-$In_{0.42}Ga_{0.58}N$ tunnel junction nanowire photocathode. Shown in Fig. 5a, the H_2 evolution in 0.5 M H_2SO_4 solution was measured as a function of time at a constant photocurrent density of ~12 mA cm^{-2} under AM 1.5 G one-sun illumination. The applied bias stays nearly constant at ~0 V vs. RHE, illustrated in Fig. 5a. The calculated H_2 evolution based on Faraday's law of electrolysis,

$$\text{Faradaic efficiency}(\%) = \frac{2 \times \textit{produced}\ H_2(\mathrm{mol{\cdot}cm^{-2}}) \times 96485(\mathrm{s{\cdot}A{\cdot}mol^{-1}})}{\textit{photocurrent density}(\mathrm{A{\cdot}cm^{-2}}) \times \textit{time}(\mathrm{s})} \times 100\% \quad (2)$$

It is seen that the measured (446 μmol cm^{-2}) and calculated (448.5 μmol cm^{-2}) hydrogen evolution agree well, confirming a nearly unity faradaic efficiency. The stability of *p*-$In_{0.42}Ga_{0.58}N$ tunnel junction nanowire photocathode was further evaluated by chronopotentiometry measurement [59–61], shown in Fig. 5b. A steady photocurrent density of 12 mA cm^{-2} is produced continuously at ~0 V vs. RHE without any

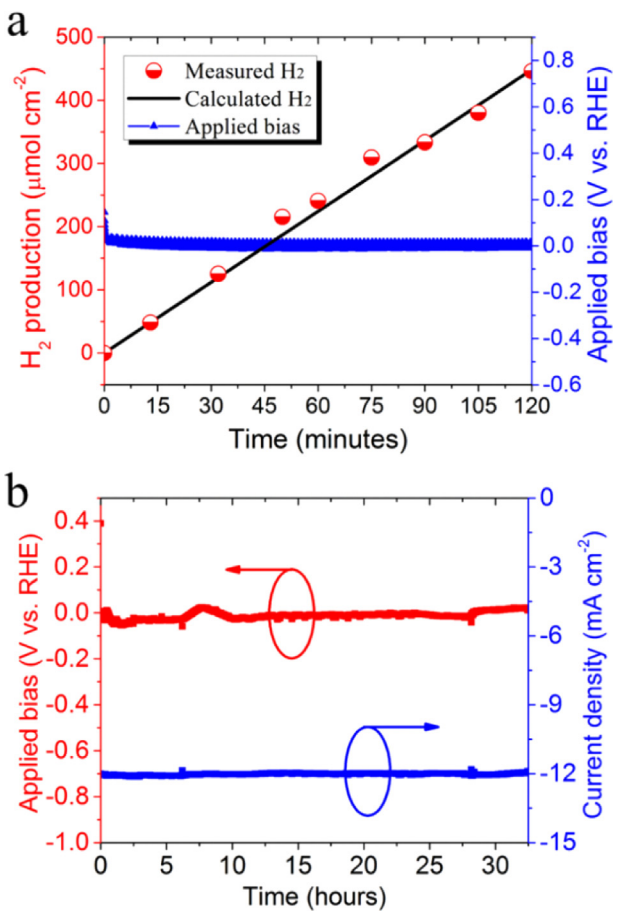

Fig. 5. Long-term stability analysis of *p*-$In_{0.42}Ga_{0.58}N$ tunnel junction nanowire photocathode measured in 0.5 M H_2SO_4 under stimulated one-sun AM 1.5 G illumination. (a) Hydrogen gas evolution under a constant photocurrent density of 12 mA cm^{-2}. The calculated H_2 production from photocurrent is also shown (solid black curve). (b) Chronopotentiometry measurement for over 30 h solar water splitting with a steady photocurrent density of 12 mA cm^{-2} at a potential of ~0 V vs. RHE.

noticeable degradation for over 30 h, demonstrating good photoelectrochemical stability of *p*-InGaN tunnel junction nanowire photocathode. For comparison, conventional Si and III-V photocathodes generally require the use of extra surface protection layer to achieve enhanced stability (see supplementary Table S2) [16,62,63].

The improved performance of *p*-InGaN tunnel junction nanowire photocathode, compared to previously reported InGaN photocathodes, is attributed to following factors: i) strongly enhanced light absorption for nanowire arrays grown on non-planar Si wafer; ii) crystalline nanowires with efficient *p*-type dopant incorporation; and iii) nanowire tunnel junctions that facilitate efficient collection of photo-excited holes and serve as an electron blocking layer to enhance the extraction of photo-excited electrons. Our recent studies have further suggested that Ga(In)N nanowire arrays grown by plasma-assisted MBE can exhibit N-terminated surfaces, not only for their top *c*-plane but also for the lateral nonpolar surfaces, which can effectively protect against photocorrosion and oxidation and therefore ensures long-term stable operation without using any extra surface protection [35].

3. Conclusion

In summary, we have investigated the fabrication and photoelectrochemical performance of a monolithically integrated *p*-InGaN tunnel junction nanowire photocathode on nonplanar Si wafer with relatively high indium composition (up to ~51%). The best performance has been achieved on a *p*-type $In_{0.42}Ga_{0.58}N$ nanowire photocathode. The open pillar design, together with the nonplanar Si wafer can significantly maximize light trapping, whereas the tunnel junction reduces the interfacial resistance and enhances the extraction of photo-generated electrons. The *p*-$In_{0.42}Ga_{0.58}N$ nanowire photocathode exhibits a photocurrent density of 12.3 mA cm^{-2} at zero bias and an onset potential of 0.79 V vs. RHE under AM 1.5G one-sun illumination. Its maximum applied bias photon-to-current efficiency reaches 4%, which is nearly one order of magnitude higher than the previously reported efficiencies of III-nitride photocathodes for solar water splitting. Significantly, no performance degradation was observed for over 30 hours solar water splitting experiment without requiring any extra surface protection, which is attributed to the spontaneous formation of N-terminated surfaces of MBE-grown GaN nanostructures to protect against photocorrosion. In addition, factors that can further improve the photoelectrode performance, such as reduced defect densities, minimized surface recombination, and more controllable formation of tunnel junction nanowires, have been identified, which, together with the integration of a buried Si p-n junction and improved charge carrier transport, promises highly efficient, stable unassisted solar water splitting and hydrogen production.

4. Experimental section

4.1. Non-planar Si surface preparation

Two-inch *n*-type silicon (100) wafer was etched in 80 °C KOH solution (1.8% KOH in weight with 20% isopropanol in volume) for 30 minutes to form the micro-textured surface. After the neutralization by hydrochloric acid, surface cleaning by acetone/methanol, and native oxide removal by 10% hydrofluoric acid, the non-planar *n*-Si wafer was then loaded into MBE chamber for III-nitride nanowires growth.

4.2. InGaN nanowire growth

p-InGaN tunnel junction nanowires were grown on as-prepared nonplanar Si substrates by plasma-assisted molecular beam epitaxy (MBE) in nitrogen-rich environment. Silicon and magnesium are used as dopants for *n*-type and *p*-type nanowire growth, respectively. Firstly, *n*-GaN nanowire template was grown for one hour with a substrate temperature of 750 °C, a gallium (Ga) beam equivalent pressure (BEP) of 8E-8 Torr, a nitrogen flow rate of 1 sccm, a plasma power of 350 W, and a silicon dopant cell temperature at 1250 °C. Then, the substrate temperature and Ga BEP were reduced to 645 °C and 3.5E-8 Torr, respectively, for the tunnel junction nanostructure, with 7 minutes n^{++}-GaN doped by silicon at 1320 °C, 2 minutes InGaN with an indium (In) BEP of 4E-8 Torr, and 10 minutes p^{++}-GaN doped by magnesium at 210 °C. Subsequently, *p*-InGaN nanowires were grown for 4 hours with Ga BEP of 2.5E-8 Torr and In BEP of 8E-8 Torr, with varied substrate temperatures and Mg doping for different indium incorporation.

4.3. Pt nanoparticle deposition

Platinum cocatalyst nanoparticles were photodeposited on *p*-InGaN nanowires in a vacuum chamber with 55 ml deionized water, 11 ml methanol, and 20 μl H_2PtCl_6 precursor solution (0.2 M conc.). InGaN nanowires were then irradiated by 300 W Xenon lamp through a quartz lid for 30 minutes.

4.4. Photoelectrochemical measurements

Photoelectrochemical measurements were conducted in a typical three-electrode configuration with a platinum counter electrode and a Ag/AgCl reference electrode in 0.5 M H_2SO_4 electrolyte solution equipped with a Newport solar simulator with AM 1.5 G filter and one-sun intensity. A BioLogic potentiostat was used to perform the PEC

measurements including linear sweep voltammetry, chronopotentiometry, and Mott-Schottky test. The production of hydrogen gas from solar water splitting on InGaN nanowires was analyzed by injecting 1 ml gas sampling into a Shimazdu gas chromatograph. The sample size is ~0.1 cm^2 for PEC measurements. It is important to note that large size samples should be demonstrated for practical solar water splitting devices in future, by further improving the growth uniformity on nonplanar Si wafers.

4.5. Structural and optical characterization

Room-temperature photoluminescence measurements of InGaN nanowires were performed in a homemade setup with a He-Cd 325 nm laser as the excitation source, and the emission is spectrally resolved by a SPEX spectrometer equipped with a photomultiplier detector. SEM images were recorded with a secondary electron detector using a Tescan MIRA3 system (15 kV) and a JEOL IT500 system (20 kV) with an EDX detector. High angle annular dark-field scanning transmission electron microscopy (HAADF-STEM) images were collected using a JEOL 3100R05 microscope with Cs aberration corrected STEM (300 keV, 29 mrad). STEM-EELS mapping and spectra were acquired by a Gatan quantum energy filter, at 0.25 eV per channel to capture the In and N edges simultaneously. Samples for STEM and EELS measurements were prepared in cross-section by mechanical wedge polishing that provides a large and thin area for analyzing samples in nano- and atomic scale.

Acknowledgements

The authors gratefully acknowledge research support from the HydroGEN Advanced Water Splitting Materials Consortium, established as part of the Energy Materials Network under the U.S. Department of Energy, Office of Energy Efficiency and Renewable Energy, Fuel Cell Technologies Office, under Award Number DE-EE0008086 and National Science Foundation (Grant CBET 1804458). The authors also acknowledge financial support from the University of Michigan College of Engineering and technical support from the Michigan Center for Materials Characterization. R.H. recognizes support from DOE Office of Science (DE-SC0011385). R.F. and Y.Z. thank the Chinese Scholarship Council (CSC) for the support to study at the University of Michigan. The authors wish to thank Dr. Xianghua Kong and Prof. Hong Guo at McGill University for discussions about N-surfaces of InGaN nanowires. The authors also wish to thank Reed Yalisove for assistance with sample preparation for electron microscopy.

Conflict of interest

The authors declare no competing financial interests.

Appendix A. Supporting information

Supplementary data associated with this article can be found in the online version at doi:10.1016/j.nanoen.2018.12.067.

References

[1] J.L. Young, M.A. Steiner, H. Döscher, R.M. France, J.A. Turner, Todd G. Deutsch, Direct solar-to-hydrogen conversion via inverted metamorphic multi-junction semiconductor architectures, Nat. Energy 2 (2017) 17028.
[2] W. Yang, J. Ahn, Y. Oh, J. Tan, H. Lee, J. Park, H.-C. Kwon, J. Kim, W. Jo, J. Kim, J. Moon, Adjusting the anisotropy of 1D Sb_2Se_3 nanostructures for highly efficient photoelectrochemical water splitting, Adv. Energy Mater. (2018) 1702888.
[3] J. Su, T. Minegishi, K. Domen, Efficient hydrogen evolution from water using CdTe photocathodes under simulated sunlight, J. Mater. Chem. A 5 (2017) 13154–13160.
[4] A. Fujishima, K. Honda, Electrochemical photolysis of water at a semiconductor electrode, Nature 238 (1972) 37.
[5] S. Chu, S. Vanka, Y. Wang, J. Gim, Y. Wang, Y.-H. Ra, R. Hovden, H. Guo, I. Shih, Z. Mi, Solar water oxidation by an InGaN nanowire photoanode with a bandgap of 1.7 eV, ACS Energy Lett. 3 (2018) 307–314.
[6] C. Sheng, L. Wei, Y. Yanfa, H. Thomas, S. Ishiang, W. Dunwei, M. Zetian, Roadmap on solar water splitting: current status and future prospects, Nano Futures 1 (2017) 022001.
[7] M.G. Kibria, Z. Mi, Artificial photosynthesis using metal/nonmetal-nitride semiconductors: current status, prospects, and challenges, J. Mater. Chem. A 4 (2016) 2801–2820.
[8] F.A. Chowdhury, Z. Mi, M.G. Kibria, M.L. Trudeau, Group III-nitride nanowire structures for photocatalytic hydrogen evolution under visible light irradiation, APL Mater. 3 (2015) 104408.
[9] G. Wang, Y. Ling, H. Wang, L. Xihong, Y. Li, Chemically modified nanostructures for photoelectrochemical water splitting, J. Photochem. Photobiol. C. 19 (2014) 35–51.
[10] D. Jing, L. Guo, L. Zhao, X. Zhang, H. Liu, M. Li, S. Shen, G. Liu, X. Hu, X. Zhang, K. Zhang, L. Ma, P. Guo, Efficient solar hydrogen production by photocatalytic water splitting: from fundamental study to pilot demonstration, Int. J. Hydrog. Energy 35 (2010) 7087–7097.
[11] M. Gopalakrishnan, S. Gopalakrishnan, G.M. Bhalerao, K. Jeganathan, Multiband InGaN nanowires with enhanced visible photon absorption for efficient photoelectrochemical water splitting, J. Power Sources 337 (2017) 130–136.
[12] D. Kang, J.L. Young, H. Lim, W.E. Klein, H. Chen, Y. Xi, B. Gai, T.G. Deutsch, J. Yoon, Printed assemblies of GaAs photoelectrodes with decoupled optical and reactive interfaces for unassisted solar water splitting, Nat. Energy 2 (2017) 17043.
[13] Y. Lin, R. Kapadia, J. Yang, M. Zheng, K. Chen, M. Hettick, X. Yin, C. Battaglia, I.D. Sharp, J.W. Ager, A. Javey, Role of TiO_2 surface passivation on improving the performance of p-InP photocathodes, J. Phys. Chem. C. 119 (2015) 2308–2313.
[14] R. Fan, W. Dong, L. Fang, F. Zheng, M. Shen, More than 10% efficiency and one-week stability of Si photocathodes for water splitting by manipulating the loading of the Pt catalyst and TiO2 protective layer, J. Mater. Chem. A 5 (2017) 18744–18751.
[15] J. Gu, Y. Yan, J.L. Young, K.X. Steirer, N.R. Neale, J.A. Turner, Water reduction by a p-$GaInP_2$ photoelectrode stabilized by an amorphous TiO_2 coating and a molecular cobalt catalyst, Nat. Mater. 15 (2015) 456.
[16] S. Hu, M.R. Shaner, J.A. Beardslee, M. Lichterman, B.S. Brunschwig, N.S. Lewis, Amorphous TiO_2 coatings stabilize Si, GaAs, and GaP photoanodes for efficient water oxidation, Science 344 (2014) 1005.
[17] S. Fan, I. Shih, Z. Mi, A monolithically integrated InGaN Nanowire/Si tandem photoanode approaching the ideal bandgap configuration of 1.75/1.13 eV, Adv. Energy Mater. 7 (2017) 1600952.
[18] K.T. Fountaine, H.J. Lewerenz, H.A. Atwater, Efficiency limits for photoelectrochemical water-splitting, Nat. Commun. 7 (2016) 13706.
[19] A.B. Laursen, S. Kegnaes, S. Dahl, I. Chorkendorff, Molybdenum sulfides-efficient and viable materials for electro - and photoelectrocatalytic hydrogen evolution, Energy Environ. Sci. 5 (2012) 5577–5591.
[20] S. Zhao, H.P.T. Nguyen, M.G. Kibria, Z. Mi, III-Nitride nanowire optoelectronics, Prog. Quantum Electron. 44 (2015) 14–68.
[21] Y. Dong, B. Tian, T.J. Kempa, C.M. Lieber, Coaxial group III−nitride nanowire photovoltaics, Nano Lett. 9 (2009) 2183–2187.
[22] J. Kamimura, P. Bogdanoff, J. Lähnemann, C. Hauswald, L. Geelhaar, S. Fiechter, H. Riechert, Photoelectrochemical properties of (In,Ga)N nanowires for water splitting investigated by in situ electrochemical mass spectroscopy, J. Am. Chem. Soc. 135 (2013) 10242–10245.
[23] C. Hahn, A.A. Cordones, S.C. Andrews, H. Gao, A. Fu, S.R. Leone, P. Yang, Effect of thermal annealing in ammonia on the properties of InGaN nanowires with different indium concentrations, J. Phys. Chem. C. 117 (2013) 3627–3634.
[24] S. Zhao, O. Salehzadeh, S. Alagha, K.L. Kavanagh, S.P. Watkins, Z. Mi, Probing the electrical transport properties of intrinsic InN nanowires, Appl. Phys. Lett. 102 (2013) 073102.
[25] M. Sun, Y. Zhang, X. Gao, T. Palacios, High-performance GaN vertical fin power transistors on bulk GaN substrates, IEEE Electron Device Lett. 38 (2017) 509–512.
[26] A. Stockman, M. Uren, A. Tajalli, M. Meneghini, B. Bakeroot, P. Moens, in: Proceedings of the 47th European Solid-State Device Research Conference (ESSDERC), 2017, pp. 130–133.
[27] N. Ikeda, Y. Niiyama, H. Kambayashi, Y. Sato, T. Nomura, S. Kato, S. Yoshida, GaN power transistors on Si substrates for switching applications, Proc. IEEE 98 (2010) 1151–1161.
[28] A. Nakamura, M. Suzuki, K. Fujii, Y. Nakano, M. Sugiyama, Low-temperature growth of AlN and GaN by metal organic vapor phase epitaxy for polarization engineered water splitting photocathode, J. Cryst. Growth 464 (2017) 180–184.
[29] V. Ganesh, M. Alizadeh, A. Shuhaimi, A. Adreen, A. Pandikumar, M. Jayakumar, N.M. Huang, R. Ramesh, K. Baskar, S.A. Rahman, Correlation between indium content in monolithic InGaN/GaN multi quantum well structures on photoelectrochemical activity for water splitting, J. Alloy. Compd. 706 (2017) 629–636.
[30] V. Parameshwaran, C. Gallinat, R.W. Enck, A.V. Sampath, P.H. Shen, T. Kuykendall, S. Aloni, M. Wraback, B.M. Clemens, III-V nitride semiconductors for solar hydrogen production, SPIE, 2012, p. 7, https://doi.org/10.1117/12.925200 〈https://spie.org/Publications/Proceedings/Paper/10.1117/12.925200〉.
[31] S. Zhao, Z. Mi, Recent advances on p-type III-nitride nanowires by molecular beam epitaxy, Cryst 7 (2017) 268.
[32] K. Sasamoto, T. Hotta, K. Sugita, A.G. Bhuiyan, A. Hashimoto, A. Yamamoto, K. Kinoshita, Y. Kohji, MOVPE growth of high quality p-type InGaN with intermediate in compositions, J. Cryst. Growth 318 (2011) 492–495.
[33] P.-C. Chen, C.-H. Chen, S.-J. Chang, Y.-K. Su, P.-C. Chang, B.-R. Huang, High hole concentration of p-type InGaN epitaxial layers grown by MOCVD, Thin Solid Films 498 (2006) 113–117.
[34] C.J. Eiting, P.A. Grudowski, R.D. Dupuis, P- and N-type doping of GaN and AlGaN epitaxial layers grown by metalorganic chemical vapor deposition, J. Electron.

Mater. 27 (1998) 206–209.
[35] M.G. Kibria, R. Qiao, W. Yang, I. Boukahil, X. Kong, F.A. Chowdhury, M.L. Trudeau, W. Ji, H. Guo, F.J. Himpsel, L. Vayssieres, Z. Mi, Atomic-scale origin of long-term stability and high performance of p-GaN nanowire arrays for photocatalytic overall pure water splitting, Adv. Mater. 28 (2016) 8388–8397.
[36] H. Kaneko, T. Minegishi, K. Domen, Recent progress in the surface modification of photoelectrodes toward efficient and stable overall water splitting, Chemistry–A Eur. J. 23 (2017) (n/a-n/a).
[37] T. Kuykendall, P. Ulrich, S. Aloni, P. Yang, Complete composition tunability of InGaN nanowires using a combinatorial approach, Nat. Mater. 6 (2007) 951.
[38] M. Ebaid, D. Priante, G. Liu, C. Zhao, M. Sharizal Alias, U. Buttner, T. Khee Ng, T. Taylor Isimjan, H. Idriss, B.S. Ooi, Unbiased photocatalytic hydrogen generation from pure water on stable Ir-treated $In_{0.33}Ga_{0.67}N$ nanorods, Nano Energy 37 (2017) 158–167.
[39] S. Zhao, S.M. Sadaf, S. Vanka, Y. Wang, R. Rashid, Z. Mi, Sub-milliwatt AlGaN nanowire tunnel junction deep ultraviolet light emitting diodes on silicon operating at 242 nm, Appl. Phys. Lett. 109 (2016) 201106.
[40] S.M. Sadaf, Y.H. Ra, H.P.T. Nguyen, M. Djavid, Z. Mi, Alternating-current InGaN/GaN tunnel junction nanowire white-light emitting diodes, Nano Lett. 15 (2015) 6696–6701.
[41] C.X. Ren, Polarisation fields in III-nitrides: effects and control, Mater. Sci. Technol. 32 (2016) 418–433.
[42] P. Bhattacharya, Semiconductor Optoelectronic Devices, second ed., Pearson Education Inc., New Jersey, 1996.
[43] R. Belghouthi, M.H. Gazzah, H. Mejri, in: Proc. International Conference on Green Energy Conversion Systems (GECS) 2017, 2017, pp. 1–6.
[44] S. Fan, B. AlOtaibi, S.Y. Woo, Y. Wang, G.A. Botton, Z. Mi, High efficiency solar-to-hydrogen conversion on a monolithically integrated InGaN/GaN/Si adaptive tunnel junction photocathode, Nano Lett. 15 (2015) 2721–2726.
[45] S. Krishnamoorthy, F. Akyol, P.S. Park, S. Rajan, Low resistance GaN/InGaN/GaN tunnel junctions, Appl. Phys. Lett. 102 (2013) 113503.
[46] M.G. Kibria, F.A. Chowdhury, S. Zhao, B. AlOtaibi, M.L. Trudeau, H. Guo, Z. Mi, Visible light-driven efficient overall water splitting using p-type metal-nitride nanowire arrays, Nat. Commun. 6 (2015) 6797.
[47] S. Chu, X. Kong, S. Vanka, H. Guo, Z. Mi, Chapter six - artificial photosynthesis on iii-nitride nanowire arrays, in: Z. Mi, L. Wang, C. Jagadish (Eds.), Semiconductors and Semimetals, Elsevier, 2017, pp. 223–255.
[48] C. Liu, N.P. Dasgupta, P. Yang, Semiconductor Nanowires for Artificial Photosynthesis, Chem. Mater. 26 (2014) 415–422.
[49] M.D. Kelzenberg, S.W. Boettcher, J.A. Petykiewicz, D.B. Turner-Evans, M.C. Putnam, E.L. Warren, J.M. Spurgeon, R.M. Briggs, N.S. Lewis, H.A. Atwater, Enhanced absorption and carrier collection in Si wire arrays for photovoltaic applications, Nat. Mater. 9 (2010) 239.
[50] R.R. Pelá, C. Caetano, M. Marques, L.G. Ferreira, J. Furthmüller, L.K. Teles, Accurate band gaps of AlGaN, InGaN, and AlInN alloys calculations based on LDA-1/2 approach, Appl. Phys. Lett. 98 (2011) 151907.
[51] I. Vurgaftman, J.R. Meyer, Band parameters for nitrogen-containing semiconductors, J. Appl. Phys. 94 (2003) 3675–3696.
[52] J. Kang, Q. Huang, A broad photoluminescence band in heavily Ge-doped GaAs grown by the liquid-encapsulated Czochralski technique, J. Appl. Phys. 76 (1994) 5927–5930.
[53] S.Y. Woo, M. Bugnet, H.P.T. Nguyen, Z. Mi, G.A. Botton, Atomic ordering in InGaN alloys within nanowire heterostructures, Nano Lett. 15 (2015) 6413–6418.
[54] R.T. ElAfandy, M. Ebaid, J.-W. Min, C. Zhao, T.K. Ng, B.S. Ooi, Flexible InGaN nanowire membranes for enhanced solar water splitting, Opt. Express 26 (2018) A640–A650.
[55] S. Eftychis, J. Kruse, T. Koukoula, T. Kehagias, P. Komninou, A. Adikimenakis, K. Tsagaraki, M. Androulidaki, P. Tzanetakis, E. Iliopoulos, A. Georgakilas, Understanding the effects of Si (111) nitridation on the spontaneous growth and properties of GaN nanowires, J. Cryst. Growth 442 (2016) 8–13.
[56] H. Bazrafshan, R. Shajareh Touba, Z. Alipour Tesieh, S. Dabirnia, B. Nasernejad, Hydrothermal synthesis of Co_3O_4 nanosheets and its application in photoelectrochemical water splitting, Chem. Eng. Commun. 204 (2017) 1105–1112.
[57] T. Wang, Y. Wei, X. Chang, C. Li, A. Li, S. Liu, J. Zhang, J. Gong, Homogeneous Cu_2O p-n junction photocathodes for solar water splitting, Appl. Catal. B 226 (2018) 31–37.
[58] M. Patel, M. Kumar, J. Kim, Y.K. Kim, Photocurrent enhancement by a rapid thermal treatment of Nanodisk-shaped SnS photocathodes, J. Phys. Chem. Lett. (2017) 6099–6105.
[59] W. Vijselaar, P. Westerik, J. Veerbeek, R.M. Tiggelaar, E. Berenschot, N.R. Tas, H. Gardeniers, J. Huskens, Spatial decoupling of light absorption and catalytic activity of Ni–Mo-loaded high-aspect-ratio silicon microwire photocathodes, Nat. Energy 3 (2018) 185–192.
[60] M. Gong, W. Zhou, M.J. Kenney, R. Kapusta, S. Cowley, Y. Wu, B. Lu, M.-C. Lin, D.-Y. Wang, J. Yang, B.-J. Hwang, H. Dai, Blending Cr_2O_3 into a NiO–Ni electrocatalyst for sustained water splitting, Angew. Chem. Int. Ed. 127 (2015) 12157–12161.
[61] M.J. Kenney, M. Gong, Y. Li, J.Z. Wu, J. Feng, M. Lanza, H. Dai, High-performance silicon photoanodes passivated with ultrathin nickel films for water oxidation, Science 342 (2013) 836.
[62] J. Gu, J.A. Aguiar, S. Ferrere, K.X. Steirer, Y. Yan, C. Xiao, James L. Young, M. Al-Jassim, N.R. Neale, J.A. Turner, A graded catalytic–protective layer for an efficient and stable water-splitting photocathode, Nat. Energy 2 (2017) 16192.
[63] M.R. Shaner, S. Hu, K. Sun, N.S. Lewis, Stabilization of Si microwire arrays for solar-driven H_2O oxidation to O_2(g) in 1.0 M KOH(aq) using conformal coatings of amorphous TiO_2, Energy Environ. Sci. 8 (2015) 203–207.

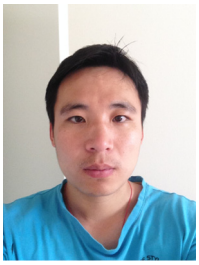

Yongjie Wang is a Ph.D. student in Electrical and Computer Engineering at the University of Michigan. He received his B.E. degree in 2012 from Composite Materials and Engineering, Harbin Institute of Technology, China, and M.S. degree from the University of California in 2014. His current research focuses on photocatalytic and photoelectrochemical water splitting on III-nitride and TMDC nanostructures.

Srinivas Vanka is a Ph.D. student in Electrical and Computer Science department at McGill University. He received his B.E. degree in Electronics and Electrical Communication, and M.Sc. degree in Chemistry from BITS Pilani, Hyderabad Campus in 2013. His current research is related to photoelectrochemical water splitting and photocatalytic carbon dioxide reduction using III-nitride nanostructures.

Jiseok Gim is currently a Ph.D student in the Materials Science & Engineering Department at University of Michigan, Ann Arbor. He received his B.S. degree in 2012 and M.E. degree in 2014 in Materials Science and Engineering from Korea University (Seoul, South Korea). His research uses high-resolution scanning transmission electron microscopy to study the structure of group III-nitride nanostructures.

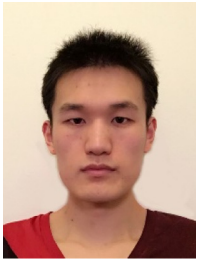

Yuanpeng Wu is a Ph.D. student in Electrical and Computer Engineering at the University of Michigan, Ann Arbor. He received his B.S. degree in 2012 from Shanxi University and M.E. degree from Zhejiang University in 2015 in China. His current research focuses on III-nitride nanostructure growth, characterization and high performance deep UV optoelectronic devices.

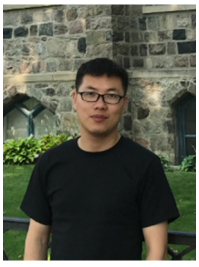

Ronglei Fan is currently a Ph.D. student at College of Physics, Soochow University, supervised by Prof. Mingrong Shen. From 2017–2018, he studied as a joint Ph.D. student in Prof. Zetian Mi's research group at Electrical Engineering and Computer Science, University of Michigan, Ann Arbor. He received his B.E. and M.S. degrees in 2013 and 2016 from Soochow University. His research focuses on the design of Si based photoelectrodes for photoelectrochemical (PEC) water splitting.

Yazhou Zhang is a Ph.D student in Power Engineering and Engineering Thermophysics at Xi'an Jiaotong University, Xi'an, China. He received his B.E. degree in 2013 from Optical Information Science and Technology at the same university. He was a visiting student under the supervision of Prof. Zetian Mi at the University of Michigan in 2017–2018. His research interest is focused on photocatalytic and photoelectrochemical properties on perovskite oxynitride and metal-free graphitic carbon nitride as well as development of novel visible-light-driven photocatalysts for water splitting.

Jinwen Shi is an associate professor at the International Research Center for Renewable Energy, State Key Laboratory of Multiphase Flow in Power Engineering, and at the Department of New Energy Science and Engineering, School of Energy and Power Engineering, Xi'an Jiaotong University, Xi'an, China. His research interest is focused on the conversion and utilization of renewable energies, new energy materials, and photocatalysis, especially the development of novel photocatalysts and photocatalytic systems for water splitting under visible-light irradiation. He published nearly 50 SCI-indexed papers in international journals and applied for 7 China invention patents.

Mingrong Shen is a Professor of College of Physics, Soochow University, China. He received a Ph.D. degree in 1997 from Institute of Plasma Physics, Chinese Academy of Sciences. He is the Director of Jiangsu Key Laboratory of Thin Film Materials and the Vice President of Jiangsu Physics Society. His group mainly focuses on the preparation and physical properties of ferroelectric thin films, inorganic multifunctional materials, especially energy-related materials. He has published more than 140 SCI papers in peer reviewed scientific journals with over 1600 citations. The H-index is 22.

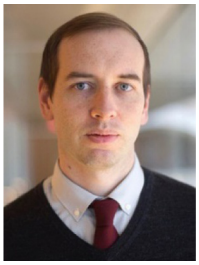

Robert Hovden is an assistant professor in the Materials Science & Engineering Department and the Applied Physics Program at the University of Michigan. He received his Ph.D. in Applied Physics at Cornell University in 2014. His research focuses on novel techniques to probe atomic structure and its properties using high energy electron beams.

Zetian Mi is a Professor in the Department of Electrical Engineering and Computer Science at the University of Michigan. He received the Ph.D. in Applied Physics from the University of Michigan in 2006. His research interests are in the areas of III-nitride semiconductors, low dimensional nanostructures, LEDs, lasers, quantum photonics, and solar fuels. He has received the Young Scientist Award from the Int. Symp. on Compound Semiconductors and the Young Investigator Award from the 27th North American Molecular Beam Epitaxy Conference. He is a Fellow of SPIE and OSA.